Condensed Matter and Interphases. 2024;26(3): 3407–416

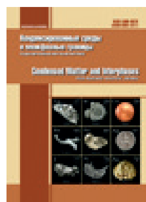

ISSN 1606-867X (Print)
ISSN 2687-0711 (Online)
Condensed Matter and Interphases
Kondensirovannye Sredy i Mezhfaznye Granitsy
https://journals.vsu.ru/kcmf/

Original articles

Research article
https://doi.org/10.17308/kcmf.2024.26/12215

Formation of silver nanocrystals in Ag-Si composite films obtained by ion beam sputtering

K. A. Barkov[1]✉, V. A. Terekhov[1], D. N. Nesterov[1], K. E. Velichko[1,2], S. A. Ivkov[1], N. S. Buylov[1,2], S. V. Kannykin[1], I. E. Zanin[1], B. V. Agapov[1,2], S. V. Rodivilov[2], E. S. Kersnovsky[1], I. V. Polshin[1], S. V. Ryabtsev[1], M. V. Grechkina[1], A. V. Sitnikov[3]

[1]*Voronezh State University,*
1 Universitetskaya pl., Voronezh 394018, Russian Federation

[2]*Research Institute of Electronic Technology,*
5 Staryh Bolshevikov st., Voronezh 394033, Russian Federation

[3]*Voronezh State Technical University,*
84 20 letiya Oktyabrya st., Voronezh 394006, Russian Federation

Abstract

Nanostructured composite films based on Ag-Si containing silver nanoparticles are used as a material for SERS (Surface-enhanced Raman spectroscopy) substrates, plasmonic back reflector, nanoplasmonic sensors, nonlinear optics devices, memristor structures, etc. Due to the widespread use of nanocomposite films based on Ag-Si, there is a need to develop simple and affordable methods for their production compatible with semiconductor technology. Therefore, this work is devoted to the production of an $Ag_{80}Si_{20}$ nanocomposite film with a high silver content (80 at.%) by ion-beam sputtering with simultaneous control of the morphology, structure, phase composition and electrical properties of the manufactured sample. As a result of complex studies using X-ray diffraction, ultra-soft X-ray emission spectroscopy, SEM and AFM microscopy, it was found that the film is a nanocomposite material based on silver nanoparticles with an average size of ~15÷30 nm. At the same time, some silver nanoparticles are in direct contact, while some Ag nanoparticles are isolated from each other by a shell of silicon dioxide SiO_2 and amorphous silicon *a*-Si. Such a nanogranulated structure of the $Ag_{80}Si_{20}$ film causes the presence in the test sample of the effect of switching from a high-resistance state (880 Ohm) to a low-resistance state (~1 Ohm) under the action of a voltage of ~ 0.2 V. As a result of the formation of conductive filaments (CF) of Ag atoms in the dielectric layer between the silver granules.

Keywords: Silver nanoparticles, Ag NPs, Ag-Si films, Ultra-soft X-ray emission spectroscopy, Ion-beam sputtering

Funding: This work was funded by the Russian Science Foundation, under grant number 23-79-10294, https://rscf.ru/project/23-79-10294/

Acknowledgments: The research results were partially obtained using the equipment of the Voronezh State University's Center for Collective Use. URL: http://ckp.vsu.ru

For citation: Barkov K. A., Terekhov V. A., Nesterov D. N., Velichko K. E., Ivkov S. A., Buylov N. S., Kannykin S. V., Zanin I. E., Agapov B. V., Rodivilov S. V., Kersnovsky E. S., Polshin I. V., Ryabtsev S. V., Grechkina M. V., Sitnikov A. V. Formation of silver nanocrystals in Ag-Si composite films obtained by ion beam sputtering. *Condensed Matter and Interphases*. 2024;26(3): 407–416. https://doi.org/10.17308/kcmf.2024.26/12215

Для цитирования: Барков К. А., Терехов В. А., Нестеров Д. Н., Величко К. Е., Ивков С. А., Буйлов Н. С., Канныкин С. В., Занин И. Е., Агапов Б. В., Родивилов С. В., Керсновский Е. С., Польшин И. В., Рябцев С. В., Гречкина М. В., Ситников А. В. Формирование нанокристаллов серебра в композитных пленках Ag-Si, полученных ионно-лучевым распылением. *Конденсированные среды и межфазные границы*. 2024;26(3): 407–416. https://doi.org/10.17308/kcmf.2024.26/12215

✉ Konstantin A. Barkov, e-mail: barkov@phys.vsu.ru

© Barkov K. A., Terekhov V. A., Nesterov D. N., Velichko K. E., Ivkov S. A., Buylov N. S., Kannykin S. V., Zanin I. E., Agapov B. V., Rodivilov S. V., Kersnovsky E. S., Polshin I. V., Ryabtsev S. V., Grechkina M. V., Sitnikov A. V., 2024

The content is available under Creative Commons Attribution 4.0 License.

1. Introduction

Nanostructured composite materials containing silver nanoparticles, due to their ability to amplify the electromagnetic field near the surface of metal nanoparticles when interacting with light (surface plasmon resonance), are a promising material for the manufacturing technology of SERS substrates used for high-precision diagnostics and detection of very low concentrations of material by Raman spectroscopy [1–3]. In addition, silver nanoparticles are used to create structures with a plasmonic back reflectors in order to increase the efficiency of solar cells [4,5], nanoplasmic sensors [6] and nonlinear optics devices [7,8]. In addition, silicon decorated with silver nanoparticles is considered one of the candidates as an anode material for next-generation lithium-ion batteries with high energy density [9–11]. Despite the high theoretical capacity of 4200 mA·h/g of silicon, a strong volume change (> 300%) of the silicon anode occurs during the lithiation–delithiation process, which leads to its destruction and deterioration of electrochemical characteristics. Surface nanostructuring of a silicon anode using silver nanoparticles makes it possible to improve the conductivity of a silicon anode and reduce internal stresses when the volume of silicon changes, which leads to a significant increase in electrochemical characteristics [9–11]. It was shown in [9] that when using an Ag-Si nanocomposite film with a silver content of about 20% as an anode, the Coulomb efficiency reaches 95%, due to a decrease in the polarization of the anode due to the presence of silver nanoparticles. Currently, nanostructured Ag-Si and Ag-SiO_x films are of interest for creating random access memory (RAM), since they have the effect of switching from a high-resistance to a low-resistance state (memristor effect) [12–15]. Moreover, such structures are used as artificial electrical synapses for building neuromorphic computing systems. [16–18].

The widespread use of nanocomposite films based on Ag-Si leads to the need to develop simple and affordable methods for their production compatible with semiconductor technology. At the same time, additional difficulties are in the formation of metal nanoparticles in films with a high metal content as a result of their coalescence into larger particles [19]. Therefore, this work is devoted to the production of an $Ag_{80}Si_{20}$ nanocomposite film with a high silver content (80 at.%) by ion-beam sputtering with simultaneous control of the morphology, structure, phase composition and electrical properties of the resulting sample.

2. Experimental

2.1 Preparation of the $Ag_{80}Si_{20}$ film by ion-beam sputtering

The $Ag_{80}Si_{20}$ film with a thickness of about 1.5 μm was obtained on a Si (100) substrate of the KDB-12 brand by ion-beam sputtering of a composite target (size 100x200 mm) made of pure silver Ag (99.99%) and Si (KDB-12) silicon strips with a size of 100x10 mm. To obtain the $Ag_{80}Si_{20}$ film of the desired atomic composition, silicon strips with a width of 10 mm were placed at a distance of 20 mm on the surface of the silver plate. The deposition was realized in a vacuum chamber (10^{-6} Торр) filled with Ar (purity99.992%) up to the total gas pressure $8 \cdot 10^{-4}$ Торр. A magnetic system consisting of permanent magnets, a magnetic circuit and an anode was used as a source of ion-beam sputtering. Argon ionization is carried out in the gap of the magnetic circuit located in the immediate vicinity of the anode, to which a positive displacement of 4 kV is applied. The optimal plasma current is ~170 μA. The sputtering coefficients of Ag and Si were 11.8 [20] and 1.5 [21], respectively. This mode ensures the deposition rate of the $Ag_{80}Si_{20}$ film ~1.5 μ/h. The ion beam sputtering technique is described in more detail in the works [20,21].

2.2 Methods of characterization of the $Ag_{80}Si_{20}$ ion-beam film

The atomic composition of the film was determined using a JEOL JSM-6380LV scanning electron microscope (SEM) with an INCA Energy 250 microanalysis attachment at a primary electron energy of 5 keV.

The structure of the sample was analyzed using a PANalytical Empyrean B.V. X-ray diffractometer with Cu $K\alpha_{1,2}$-radiation λ = 1.542 Å.

The surface morphology of the $Ag_{80}Si_{20}$ ion-beam film was analyzed using the Solver P47 NT-MDT scanning atomic force microscope (AFM) in the 1x1 μm scanning area.

The phase composition of the $Ag_{80}Si_{20}$ film was determined using a unique technique of ultra-soft X-ray emission spectroscopy (USXES) implemented on the RSM-500 spectrometer. This method allows recording the characteristic X-ray Si $L_{2.3}$ radiation resulting from electron transitions from the valence band to the Si 2p core level. As a result, the USXES method provides information about the density of electronic states in the valence band, which makes it possible to detect the presence of Si-Si or Si-O bonds, regardless of the degree of ordering of the atomic structure of the film [22,23]. Modeling using reference spectra makes it possible to determine the contribution of amorphous, crystalline and oxide/suboxide phases of silicon in experimental Si $L_{2.3}$-spectra [24]. The excitation of X-ray emission Si $L_{2.3}$-spectra was carried out by an electron beam with an energy E from 1 to 3 keV, which provided an analysis depth of 10 to 60 nm [25].

The electrophysical properties of the film were studied using the current-voltage characteristics (I-V) obtained using a probe installation and a digital oscilloscope Aktakom ASK-4106 in the range from -0.6 to +0.6 V.

3. Results and discussion

3.1 Surface morphology of the $Ag_{80}Si_{20}$ ion-beam film

As a result of ion-beam sputtering of a composite target based on Ag and Si, a sufficiently thick film ~ 1.6 microns thick is formed under these conditions, as can be seen in the cross section SEM image (Fig. 1a). The analysis of the elemental composition by energy dispersive spectroscopy (EDS) shows that the resulting ion-beam file has an atomic composition of Ag 79 at.% and Si 21 at.% ($Ag_{79}Si_{21}$) close to the technologically specified $Ag_{80}Si_{20}$. The elemental composition was analyzed at a primary electron energy of 5 keV in order to limit the depth of the analyzed layer to the thickness of the film. The surface of the $Ag_{80}Si_{20}$ film has a continuous and homogeneous structure (Fig. 1b). At the same time, according to AFM data, the surface of the $Ag_{80}Si_{20}$ film is granular with an average granule size of ~30 nm, which is clearly visible in the three-dimensional AFM image obtained by scanning a 1×1 μm surface area (Fig. 2a). On the surface of the $Ag_{80}Si_{20}$ film, both individual granules and conglomerates formed by these granules reaching sizes of ~100–200 nm are clearly distinguishable (Fig. 2a). The average surface roughness of the $Ag_{80}Si_{20}$ film is in the range of 2.5÷3 nm, while some local relief inhomogeneities reach a height of 40÷70 nm.

The formation of granular nanoparticles in the $Ag_{80}Si_{20}$ film is clearly visible in the AFM image obtained in phase contrast mode with a scanning area of 1×1 μm (Fig. 2b). At the same time, it is clearly visible from Fig. 2b that some nanoparticles are in direct contact, while some of the nanoparticles are surrounded by a shell with a different kind of contrast (light areas in Fig. 2b). Based on the atomic composition and AFM images of the $Ag_{80}Si_{20}$ film, it can be assumed that the nanogranules are formed on

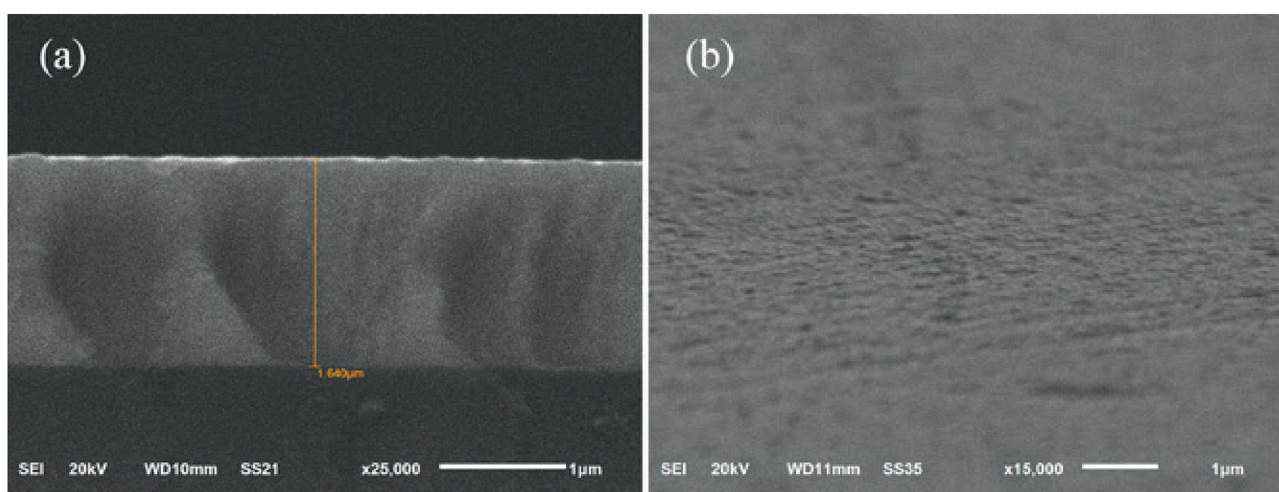

Fig. 1. SEM images of the cross section (a) and the surface (b) of the $Ag_{80}Si_{20}$ ion-beam film

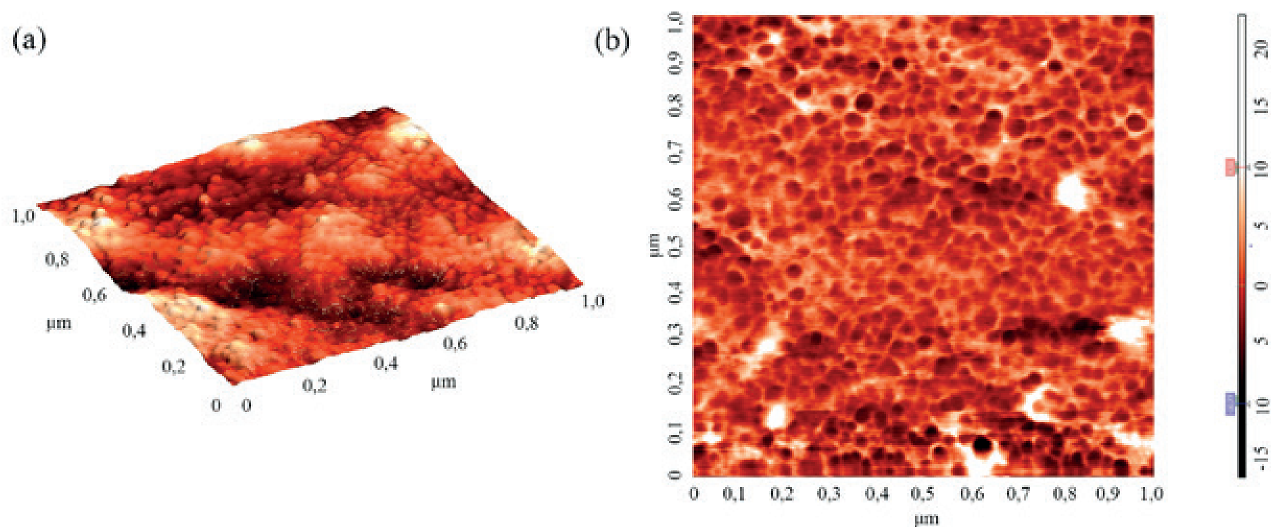

Fig. 2. Three-dimensional AFM image of the surface of the $Ag_{80}Si_{20}$ film (a) and phase contrast (b) obtained with a scanning area of 1×1 µm

the basis of silver, and the shell separating them is formed by silicon. Therefore, X-ray diffraction and X-ray spectroscopic studies were carried out to unambiguously answer the question about the phase composition of granules and shells in the $Ag_{80}Si_{20}$ film.

3.2. Structure and phase composition of the $Ag_{80}Si_{20}$ ion-beam film

Fig. 3 shows XRD patterns of the $Ag_{80}Si_{20}$ ion-beam film, as well as pure silver (99.99%) and polycrystalline silicon (poly-Si). The X-ray diffraction pattern of the $Ag_{80}Si_{20}$ ion-beam film shows XRD lines at values 2θ = 38.20°, 44.10°, 64.30°, 77.15°, corresponding to the values of *d*-spacings 2.356 Å, 2,054 Å, 1.448 Å, 1.236 Å, respectively. All of these XRD lines are associated with reflections from the crystallographic planes Ag (111), Ag (200), Ag (220), Ag (222) and Ag (400) (ICDD PDF-2, Card No. 00-004-0783). At the same time, all XRD reflexes in the $Ag_{80}Si_{20}$ film are greatly expanded compared to similar reflexes in the pure Ag standard, which indicates a small size of the crystallites. To estimate the average size of the crystallites by broadening the diffraction line, a section of the XRD pattern in the area of the Ag (111) line was recorded separately in a step-by-step mode with a long accumulation time in pure silver (Fig. 4a) and an $Ag_{80}Si_{20}$ ion-beam film (Fig. 4b). The Ag (111) XRD lines obtained in this way were decomposed on the double line Cu$K\alpha_1$, $K\alpha_2$ by Lorentz functions according to the standard procedure described in the [26–28]. Fig. 4 shows that the half-width $K\alpha_1$ of the Ag (111) reflex (0.35 *2*θ deg.) is significantly larger compared to the same reflex in pure silver (0.12 *2*θ deg.). Using the values of the half-width and position of the $K\alpha_1$ component, the average sizes of silver crystallites in the $Ag_{80}Si_{20}$ film were determined using the Debye-Scherrer formula, which amounted to ~15 nm, which is consistent with AFM data. Thus, according to the results of X-ray diffraction analysis, silver in the ion-beam film $Ag_{80}Si_{20}$ is in a nanocrystalline state. At the same time, no crystalline phases based on silicon were detected in this film according to XRD data. Therefore, further studies of the phase composition of this sample will be carried out using the USXES method.

X-ray emission Si $L_{2.3}$-spectra of the $Ag_{80}Si_{20}$ film obtained at analysis depths of 10, 35 and 60 nm are shown in Fig. 5. Two intensity peaks are observed in all X-ray spectra at E = 89 and 94.5 eV. The presence of these intensity maxima is due to the presence of Si 3*s* and O 2*p* states and is characteristic of the SiO_2 silicon dioxide spectrum [29,30], the spectrum of which is shown in the same figure for clarity. In addition, the formation of the silicon oxide phase in the $Ag_{80}Si_{20}$ film is additionally evidenced by the presence of a long-wavelength satellite in the X-ray spectrum at 77 eV. However, in all X-ray

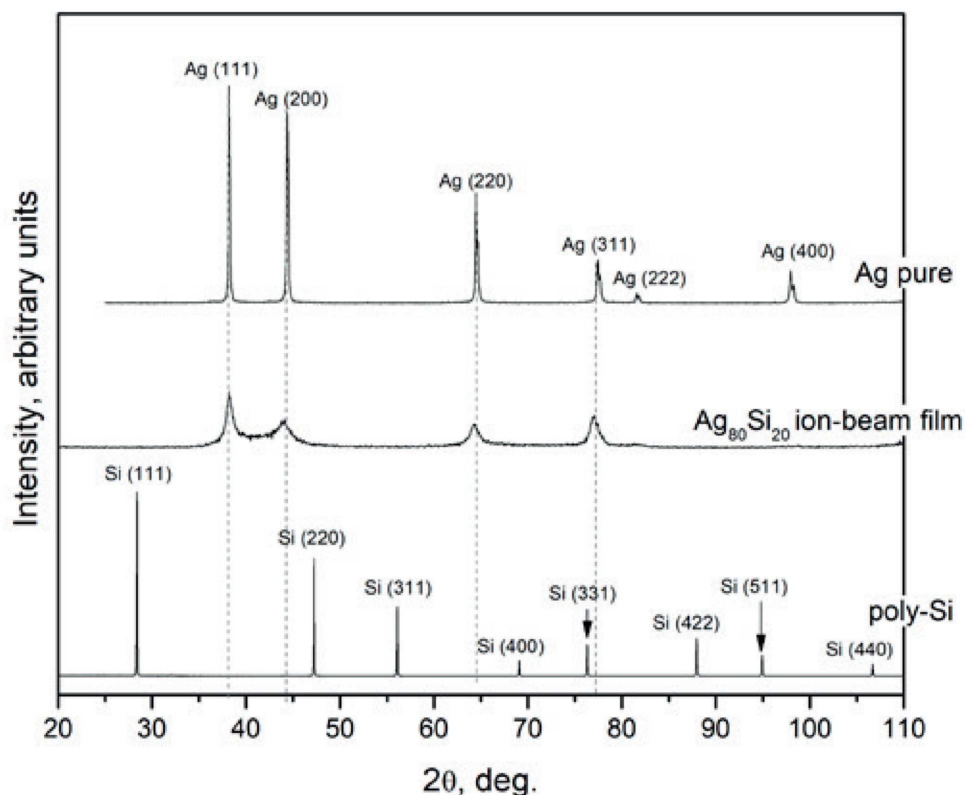

Fig. 3. XRD patterns of the $Ag_{80}Si_{20}$ ion-beam film, as well as polysilicon and pure silver standards

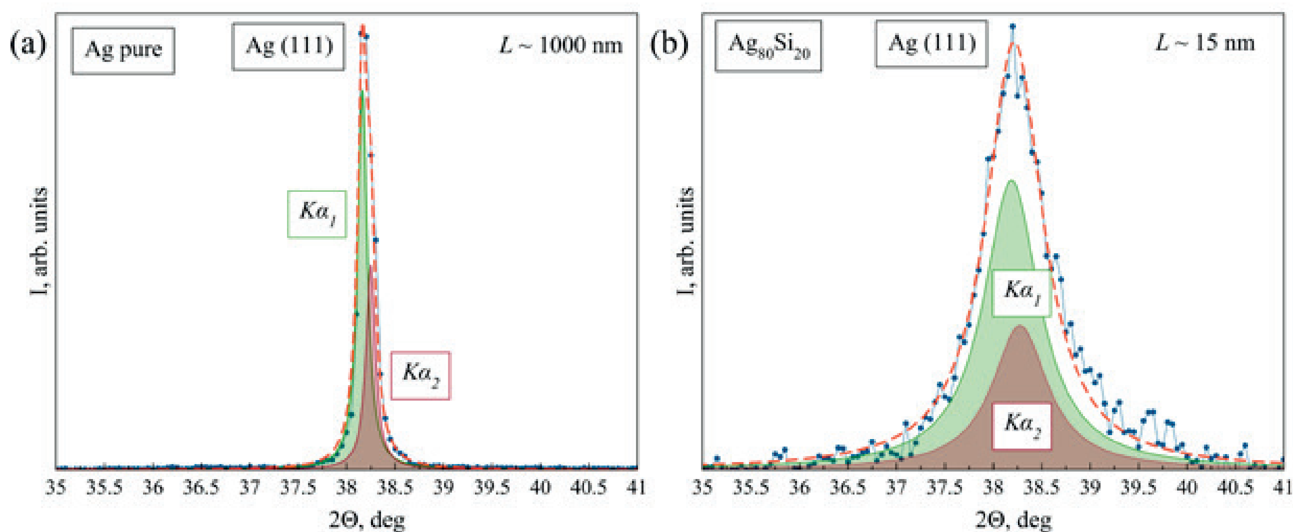

Fig. 4. XRD patterns of the $Ag_{80}Si_{20}$ ion-beam film and pure silver, recorded with a long accumulation time in the area of the Ag (111) line, as well as the result of their decomposition into components Cu$K\alpha_1$ and Cu$K\alpha_2$ by Lorentz functions

spectra of the $Ag_{80}Si_{20}$ film, the intensity in the region of 92 eV is noticeably higher compared to the SiO_2 spectrum. Such an increase in the intensity of the spectrum at 92 eV is due to the presence of a non-oxidized silicon phase in the $Ag_{80}Si_{20}$ film, the maximum of which is in this energy region. To identify the phase of non-oxidized silicon in the $Ag_{80}Si_{20}$ film, experimental X-ray spectra based on standards were simulated [24]. The simulated spectra are shown in Fig. 5 as solid red lines. The simulation results show that in the surface layer of the $Ag_{80}Si_{20}$ film

with a depth of 10 nm, silicon is indeed mainly contained in the form of the SiO_2 phase, however, part of the silicon atoms (about 10%) is in the amorphous silicon *a*-Si phase. At the same time, with an increase in the depth of analysis to 35 nm, it leads to an increase in the *a*-Si content to 35%, which may be due to a decrease in the influence of the surface oxide. A further increase in the depth of analysis to 60 nm does not lead to a change in the shape of the X-ray spectrum, which indicates the uniformity of the phase composition of the $Ag_{80}Si_{20}$ film in depth. Thus, according to X-ray diffraction and ultra-soft X-ray emission spectroscopy, the $Ag_{80}Si_{20}$ ion-beam film is a nanocomposite material containing silver nanogranules with an average size of about 15 nm, separated by a layer based on silicon dioxide and amorphous silicon.

3.3. Electrical properties of $Ag_{80}Si_{20}$ ion beam film

To study the electrical properties of the $Ag_{80}Si_{20}$ ion beam film, the current-voltage characteristics in the plane geometry of the sample were measured (Fig. 6). It can be seen from Figure 6 that with an increase in voltage from 0 to 0.6 V on the I-V characteristic in the 0.2 V region, there is an abrupt change in the recorded current values from $1.5 \cdot 10^{-4}$ to 0.1 A (by almost three orders of magnitude), the value of which increases smoothly with a further increase in the applied voltage, which is clearly visible on a logarithmic scale, shown in the box to Fig. 6. The evaluation of the resistance values *R* of the $Ag_{80}Si_{2}0$ film in two linear sections reveals the effect of switching at 0.2 V from the high-resistance state of the film (~880 Ohm) to the low-resistance (~1 Ohm). At

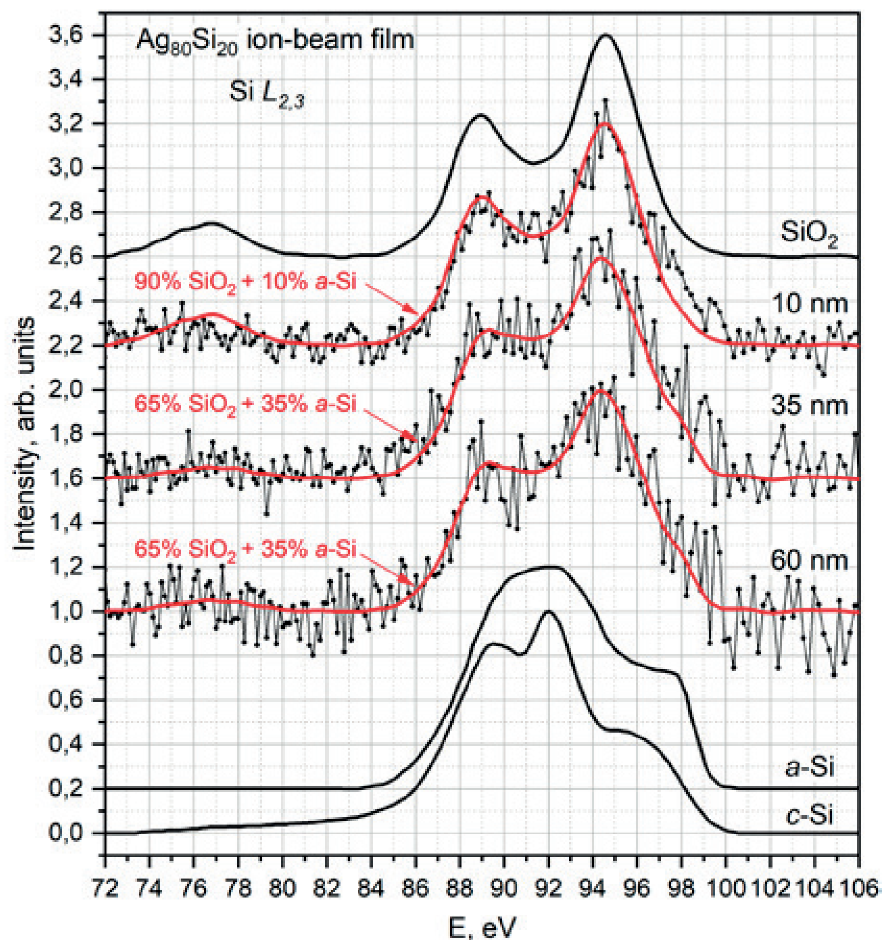

Fig. 5. X-ray emission Si $L_{2,3}$-spectra of the $Ag_{80}Si_{20}$ film obtained at analysis depths of 10, 35 and 60 nm, as well as spectra of standards of crystalline silicon (*c*-Si), amorphous silicon (*a*-Si) and silicon dioxide (SiO_2). The experimental spectrum is represented by dots, the model is represented by a solid red line

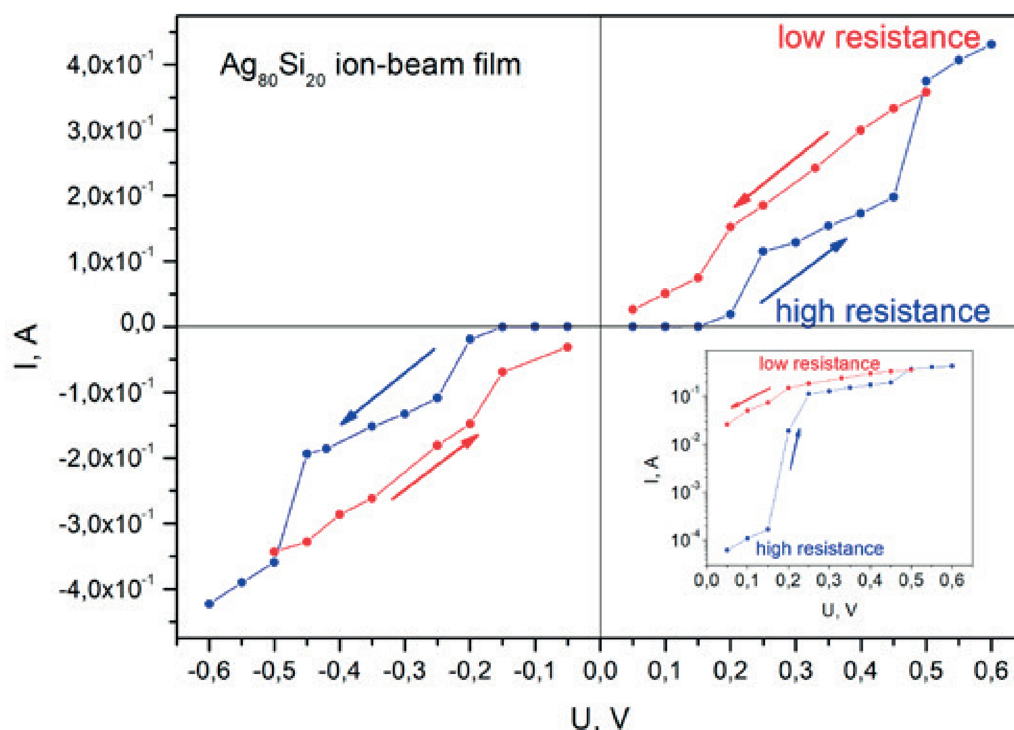

Fig. 6. Current-voltage curve of the ion beam film $Ag_{80}Si_{20}$. The insert shows a straight branch of the *I-V* curve on a logarithmic scale

the same time, in the case of a decrease in the voltage applied to the film from 0.6 to 0.05 V, the film remains in a low-resistance state until the current polarity changes, and hysteresis can be seen on the *I-V* characteristic. A similar character of the *I-V* curves was observed in the case of nanogranulated silver films obtained by thermal evaporation followed by oxidation at 100 °C [31], in Ag-SiO_2, nanocomposite films obtained by the sol-gel method with an Ag content of ~50% [14], in Ag-SiO_x nanocomposite structures [12, 13]. In such films, silver nanoparticles are mostly isolated either by an oxide layer or by a dielectric matrix, and only individual particles of the system come into contact with each other. The state of the film in which individual particles are on the verge of forming a bound system is called the percolation threshold. In such a system, switching can be associated with various mechanisms of current flow: thermally induced tunneling at low fields, and field-induced tunneling at high fields [14, 32]. On the other hand, the switching effect may be associated with the formation of conductive filaments (CF) in the dielectric layer (in our case SiO_2 + *a*-Si) between the silver granules under the action of voltage [12, 13, 32]. The formation of conductive filaments in the dielectric is due to the interaction of Ag atoms on the surface of nanogranules with broken Si bonds, followed by diffusion and gradual accumulation of Ag atoms in the dielectric [13]. The second mechanism describing the switching effect in this case seems to be predominant, since the studied ion-beam film $Ag_{80}Si_{20}$ after switching to a low-resistance state does not return to a high-resistance state when the electric voltage is removed, which indicates structural changes in the film.

4. Conclusions

As a result of comprehensive studies of the morphology, structure and phase composition of the $Ag_{80}Si_{20}$ film with a high silver content (80 at.%) obtained by ion beam sputtering, it was found that the film is a nanocomposite material. According to XRD and AFM microscopy, the $Ag_{80}Si_{20}$ film is nanogranulated with an average size of silver granules ~15÷30 nm. Some silver nanoparticles are in direct contact, while some Ag nanoparticles are isolated from each other by a shell, which, according to ultra-soft X-ray emission spectroscopy, consists of silicon dioxide SiO_2 and amorphous silicon *a*-Si. At the same

time, in the surface layer of the $Ag_{80}Si_{20}$ film with a depth of 10 nm, silicon is mainly contained in the form of the SiO_2 phase, and only about 10% of silicon atoms are in the amorphous silicon *a*-Si phase. At the same time, with an increase in the depth of analysis to 35 and 60 nm leads to an increase in the content of *a*-Si up to 35%. According to USXES data, the phase composition of the $Ag_{80}Si_{20}$ ion-beam film is uniform in depth. The nanogranulated structure of the $Ag_{80}Si_{20}$ film causes the presence in the test sample of the switching effect from a high-resistance state (880 Ohm) to a low-resistance state (~1 Ohm) under the influence of a voltage of ~0.2 V. The switching effect in this case may be associated with the formation of conductive filaments of Ag atoms in the dielectric layer (in our case SiO_2 + *a*-Si) between the silver granules.

Contribution of the authors

The authors contributed equally to this article.

Conflict of interests

The authors declare that they have no known competing financial interests or personal relationships that could have influenced the work reported in this paper.

References

1. Dzhagan V., Mazur N., Kapush O., ... Yukhymchuk V. Self-organized SERS substrates with efficient analyte enrichment in the hot Spots. *ACS Omega*. 2024;9(4): 4819–4830. https://doi.org/10.1021/acsomega.3c08393

2. Ermina A. A., Solodovchenko N. S., Levitskii V. S., ... Zharova Y. A. Plasmonic disordered array of hemispherical AgNPs on SiO_2@c-Si: their optical and SERS properties. *Materials Science in Semiconductor Processing*. 2024;169: 107861. https://doi.org/10.1016/j.mssp.2023.107861

3. Yang Z. W., Meng L. Y., Lin J. S., ... Li J. F. 3D hotspots platform for plasmon enhanced Raman and second harmonic generation spectroscopies and quantitative analysis. *Advanced Optical Materials*. 2019;7: 3–8. https://doi.org/10.1002/adom.201901010

4. Morawiec S., Mendes M. J., Priolo F., Crupi I. Plasmonic nanostructures for light trapping in thin-film solar cells. *Materials Science in Semiconductor Processing*. 2019;92: 10–18. https://doi.org/10.1016/j.mssp.2018.04.035

5. Atwater H. A., Polman A. Plasmonics for improved photovoltaic devices. *Nature Materials*. 2010;9: 205–213. https://doi.org/10.1038/nmat2629

6. Cesca T., Michieli N., Kalinic B., Balasa I. G., Rangel-Rojo R., Reyes-Esqueda J. A., Mattei G. Bidimensional ordered plasmonic nanoarrays for nonlinear optics, nanophotonics and biosensing applications. *Materials Science in Semiconductor Processing*. 2019;92: 2–9. https://doi.org/10.1016/j.mssp.2018.03.025

7. Lippitz M., Van Dijk M. A., Orrit M. Third-harmonic generation from single gold nanoparticles. *Nano Letters*. 2005;5: 799–802. https://doi.org/10.1021/nl0502571

8. Sato R., Ohnuma M., Oyoshi K., Takeda Y. Experimental investigation of nonlinear optical properties of Ag nanoparticles: Effects of size quantization. *Physical Review B*. 2014;90: 1–6. https://doi.org/10.1103/PhysRevB.90.125417

9. Polat D. B., Eryilmaz L., Keles O. Generation of agsi film by magnetron sputtering for use As anodes in lithium ion batteries. *ECS Meeting Abstracts*. 2015;MA2015-01: 514–514. https://doi.org/10.1149/ma2015-01/2/514

10. Liu B., Xu G., Jin C., ... Zhou L. The Si/Ag_2Si/Ag particles with the enhanced mechanical contact as anode material for lithium ion batteries. *Materials Letters*. 2020;280: 128536. https://doi.org/10.1016/j.matlet.2020.128536

11. Li S., Ma W., Luo B., ... Wang L. High-performance porous silicon/nanosilver anodes from industrial low-grade silicon for lithium-ion batteries. *ACS Applied Materials and Interfaces*. 2020;12: 49080–49089. https://doi.org/10.1021/acsami.0c14157

12. Li R., Yang H., Zhang Y., ... Huang P. Physical mechanisms and enhancement of endurance degradation of SiOx:Ag-based volatile memristors. *2023 Silicon Nanoelectronics Workshop (SNW)*. 2023;40: 117–118. https://doi.org/10.23919/SNW57900.2023.10183918

13. Ding X., Huang P., Zhao Y., Feng Y., Liu L. Understanding of the volatile and nonvolatile switching in Ag-based memristors. *IEEE Transactions on Electron Devices*. 2022;69: 1034–1040. https://doi.org/10.1109/TED.2022.3144373

14. Sarkar D. K., Cloutier F., El Khakani M. A. Electrical switching in sol-gel derived Ag-SiO_2 nanocomposite thin films. *Journal of Applied Physics*. 2005;97: 2–7. https://doi.org/10.1063/1.1870112

15. Dias C., Lv H., Picos R., ...Ventura J. Bipolar resistive switching in Si/Ag nanostructures. *Applied Surface Science*. 2017;424: 122–126. https://doi.org/10.1016/j.apsusc.2017.01.140

16. Cha J. H., Yang S. Y., Oh J., ... Choi S. Y. Conductive-bridging random-access memories for emerging neuromorphic computing. *Nanoscale*. 2020;12: 14339–14368. https://doi.org/10.1039/d0nr01671c

17. Sokolov A. S., Abbas H., Abbas Y., Choi C. Towards engineering in memristors for emerging me-

mory and neuromorphic computing: a review. *Journal of Semiconductors*. 2021;42(1): 013101. https://doi.org/10.1088/1674-4926/42/1/013101

18. Raeis-Hosseini N., Lim S., Hwang H., Rho J. Reliable $Ge_2Sb_2Te_5$-integrated high-density nanoscale conductive bridge random access memory using facile nitrogen-doping strategy. *Advanced Electronic Materials*. 2018;4(11). https://doi.org/10.1002/aelm.201800360

19. Cuenya B. R. Synthesis and catalytic properties of metal nanoparticles: Size, shape, support, composition, and oxidation state effects. *Thin Solid Films*. 2010;518: 3127–3150. https://doi.org/10.1016/j.tsf.2010.01.018

20. Semenova A.A., Semenov A.P., Goodilin E.A., Semenova I.A. Synthesis of Plasmonic Photonic Crystal SiO_2–Ag Nanostructures by Ion Beam Deposition of Silver Clusters onto Silica Microspheres. *Bulletin of the Russian Academy of Sciences: Physics*. 2019; 83: 1415–1418. https://doi.org/10.3103/S1062873819110200

21. Lunin L.S., Chebotarev S.N., Pashchenko A.S., Bolobanova L.N. Ion beam deposition of photoactive nanolayers for silicon solar cells. *Inorganic Materials*. 2012; 48: 439–444. https://doi.org/10.1134/S0020168512050111

22. Saad A. M., Fedotov A. K., Fedotova J. A., … Sitnikov A. V. Characterization of $(Co_{0.45}Fe_{0.45}Zr_{0.10})_x(Al_2O_3)_{1-x}$ nanocomposite films applicable as spintronic materials. *Physica Status Solidi C*. 2006;3: 1283–1290. https://doi.org/10.1002/pssc.200563111

23. Svito I., Fedotov A. K., Koltunowicz T. N., Saad A. Hopping of electron transport in granular $Cu_x(SiO_2)_{1-x}$ nanocomposite films deposited by ion-beam sputtering. *Journal of Alloys and Compounds*. 2015;615: S371–S374. https://doi.org/10.1016/j.jallcom.2014.01.136

24. Agarwal B. K. Soft X-ray spectroscopy. *X-Ray Spectroscopy*. Springer, Berlin, Heidelberg; 1979, p. 311–330 https://doi.org/10.1007/978-3-662-14469-5_7

25. Zimmermann P., Peredkov S., Abdala P. M., … van Bokhoven J. A. Modern X-ray spectroscopy: XAS and XES in the laboratory. *Coordination Chemistry Reviews*. 2020;423: 213466. https://doi.org/10.1016/j.ccr.2020.213466

26. Terekhov V. A., Kashkarov V. M., Manukovskii E. Yu., Schukarev A. V., Domashevskaya E. P. Determination of the phase composition of surface layers of porous silicon by ultrasoft X-ray spectroscopy and X-ray photoelectron spectroscopy techniques. *Journal of Electron Spectroscopy and Related Phenomena*. 2001;114–116: 895–900. https://doi.org/10.1016/S0368-2048(00)00393-5

27. Domashevskaya E. P., Peshkov Y. A., Terekhov V. A., Yurakov Y. A., Barkov K. A. Phase composition of the buried silicon interlayers in the amorphous multilayer nanostructures $[(Co_{45}Fe_{45}Zr_{10})/a\text{-}Si{:}H]_{41}$ and $[(Co_{45}Fe_{45}Zr_{10})_{35}(Al_2O_3)_{65}/a\text{-}Si{:}H]_{41}$. *Surface and Interface Analysis*. 2018;50: 1265–1270. https://doi.org/10.1002/sia.6515

28. Langford J. I., Wilson A. J. C. Scherrer after sixty years: a survey and some new results in the determination of crystallite size. *Journal of Applied Crystallography*. 1978;11: 102–113. https://doi.org/10.1107/S0021889878012844

29. Kovba L. M., Trunov V. K. *X-ray phase analysis*. Moscow: Moscow University Publ.; 1976, 232 p. (In Russ.)

30. Jain R. A review on the development of XRD in ferrite nanoparticles. *Journal of Superconductivity and Novel Magnetism*. 2022;35: 1033–1047. https://doi.org/10.1007/s10948-022-06213-9

31. Wiech G., Feldhütter H. O., Šimůnek A. Electronic structure of amorphous SiOx:H alloy films studied by X-ray emission spectroscopy: Si K, Si L, and O K emission bands. *Physical Review B*. 1993;47: 6981–6989. https://doi.org/10.1103/PhysRevB.47.6981

32. Nekrashevich S. S., Gritsenko V. A. Electronic structure of silicon dioxide (a review). *Physics of the Solid State*. 2014;56(2): 207–222. https://doi.org/10.1134/s106378341402022x

33. Gladskikh I. A., Gushchin M. G., Vartanyan T. A. Resistance switching in Ag, Au, and Cu films at the percolation threshold. *Semiconductors*. 2018;52: 671–674. https://doi.org/10.1134/S1063782618050093

34. Vartanyan T. A., Gladskikh I. A., Leonov N. B., Przhibel'skii S. G. Fine structures and switching of electrical conductivity in labyrinth silver films on sapphire. *Physics of the Solid State*. 2014;56: 816–822. https://doi.org/10.1134/S1063783414040349

Information about the authors

Konstantin A. Barkov, Cand. Sci. (Phys.-Math.), Head of the Laboratory, Department of Solid State Physics and Nanostructures, Voronezh State University (Voronezh, Russian Federation).

https://orcid.org/0000-0001-8290-1088
barkov@phys.vsu.ru

Vladimir A. Terekhov, Dr. Sci. (Phys.-Math.), Full Professor, Department of Solid State Physics and Nanostructures, Voronezh State University (Voronezh, Russian Federation).

https://orcid.org/0000-0002-0668-4138
terekhov@phys.vsu.ru

Dmitry N. Nesterov, Cand. Sci. (Phys.-Math.), Assistant Professor, Department of Solid State Physics and Nanostructures, Voronezh State University (Voronezh, Russian Federation).

https://orcid.org/0000-0002-2462-7153
nesterov@phys.vsu.ru

Kirill E. Velichko, Process Engineer, Research Institute of Electronic Technology (Voronezh, Russian Federation).

Sergey A. Ivkov, Cand. Sci. (Phys.-Math.), Leading Electronics Engineer, Department of Solid State Physics and Nanostructures, Voronezh State University (Voronezh, Russian Federation).

https://orcid.org/0000-0003-1658-5579
ivkov@phys.vsu.ru

Nikita S. Buylov, Cand. Sci. (Phys.-Math.), Assistant Professor, Department of Solid State Physics and Nanostructures, Voronezh State University; Engineer, Research Institute of Electronic Technology (Voronezh, Russian Federation).

https://orcid.org/0000-0003-1793-4400
buylov@phys.vsu.ru

Sergey V. Kannykin, Cand. Sci. (Phys.-Math.), Assistant Professor, Department of Materials Science and the Industry of Nanosystems, Voronezh State University; Engineer, Research Institute of Electronic Technology (Voronezh, Russian Federation).

https://orcid.org/0000-0001-8756-5722
svkannykin@gmail.com

Igor E. Zanin, Cand. Sci. (Phys.-Math.), Assistant Professor, General Physics Department, Voronezh State University (Voronezh, Russian Federation).

iezan@mail.ru

Boris L. Agapov, Cand. Sci. (Tech.), Centre for Collective Use of Scientific Equipmen, Voronezh State University, Research Institute of Electronic Technology (Voronezh, Russian Federation).

b.agapov2010@yandex.ru

Sergey V. Rodivilov, Leading Process Engineer, Research Institute of Electronic Technology (Voronezh, Russian Federation).

Evgenii S. Kersnovsky, student, Department of Solid State Physics and Nanostructures, Voronezh State University (Voronezh, Russian Federation).

https://orcid.org/0009-0006-8215-6077
kersnovsky@phys.vsu.ru

Ivan V. Polshin, student, Department of Solid State Physics and Nanostructures, Voronezh State University (Voronezh, Russian Federation).

https://orcid.org/0009-0008-7639-6538
polshin@phys.vsu.ru

Stanislav V. Ryabtsev, Dr. Sci. (Phys.-Math.), Leading Researcher, Joint Scientific and Educational Laboratory "Atomic and Electronic Structure of Functional Materials" of Voronezh State University and the National Research Center "Kurchatov Institute", Voronezh State University (Voronezh, Russian Federation).

https://orcid.org/0000-0001-7635-8162
ryabtsev@phys.vsu.ru

Margarita V. Grechkina, Leading Electronics Engineer, Departments of Semiconductor Physics and Microelectronics, Voronezh State University (Voronezh, Russian Federation).

https://orcid.org/0000-0002-7873-8625
grechkina_m@mail.ru

Aleksandr V. Sitnikov, Dr. Sci. (Phys.-Math.), Full Professor, Departments of Solid-State Electronics, Voronezh State Technical University (Voronezh, Russian Federation).

https://orcid.org/0000-0002-9438-9234
sitnikov04@mail.ru

Received 09.11.2023; approved after reviewing 05.12.2023; accepted for publication 14.12.2023; published online 01.10.2024.

Translated by Konstantin Barkov